ELSEVIER

International Journal of Mass Spectrometry 216 (2002) 59–73

International Journal of Mass Spectrometry

www.elsevier.com/locate/ijms

A time-of-flight, drift cell, quadrupole apparatus for ion mobility measurements

Patrick Weis*, Stefan Gilb, Philip Gerhardt, Manfred M. Kappes

Institut für Physikalische Chemie, Universität Karlsruhe, 76128 Karlsruhe, Germany

Received 2 January 2002; accepted 17 January 2002

Abstract

We present an instrument that incorporates a combination of three different ion sources, an (upstream) time-of-flight mass spectrometer (TOFMS), an ion mobility cell and a quadrupole mass filter. The key features of our setup are a TOFMS in front of the drift cell which allows the injection of short, intense, mass selected packets into the cell and the combination of different ion sources for increased versatility. Besides a detailed description of the experimental setup, we compare it to existing ion mobility configurations and show results on fullerenes, fullerene derivatives, large inorganic complexes and metal clusters. (Int J Mass Spectrom 216 (2002) 59–73) © 2002 Published by Elsevier Science B.V.

Keywords: Ion mobility measurements; Time-of-flight mass spectrometer; Ion mobility cell

1. Introduction

In the last decades, mass spectrometric methods have achieved extremely high resolution and sensitivity. It is now possible to determine the mass of heavy ions to within 1 ppm or less. This often allows to determine the elemental composition of large molecules such as peptides by simply weighing the ions and using the fact that the exact masses of the isotopes are not integers in atomic mass units [1]. On the other hand, the structure determination of ions in the gas phase still presents one of the great challenges in mass spectrometry [2]. While in condensed phase there exist powerful tools such as X-ray crystallography or NMR-spectroscopy, in the gas phase, we have to rely on indirect methods. Even the less complicated problem of separating different isomeric forms cannot be achieved by mass spectrometry alone. In other words, if we want to know the structure of an ion in the gas phase, we have to combine mass spectrometry with other different techniques such as collision-induced dissociation [3] or ion–molecule reactions [4].

Another, more direct way to obtain such structural information is via the measurement of the ion mobility since it is directly connected to the collision cross section of the molecule. This involves the determination of the time it takes for an ion to drift through a gas filled cell guided by a static electrical field. If we compare two ions of the same mass, the larger molecule will have a longer drift time than a smaller, more compact ion. Therefore, ion mobility measurements can add a new dimension to mass spectroscopy, the dimension of shape. The ion mobility method as such has been developed long ago by Mason and McDaniel [5] and the combination of this technique

* Corresponding author.
E-mail: patrick.weis@chemie.uni-karlsruhe.de

1387-3806/02/$ – see front matter © 2002 Published by Elsevier Science B.V.
PII S1387-3806(02)00554-7

with modern mass spectrometry has been pioneered by Kemper and Bowers [6]. They used a magnetic sector field mass spectrometer prior to the mobility cell and a quadrupole mass spectrometer after the cell. This setup allowed them to use an external ion source, and have complete control of the ion mass prior and after the drift cell. Their cell was 40 mm long and operated in the 1–10 mbar pressure regime. Among other things, they investigated the electronic states of transition metals [6], structures of carbon clusters [7], the conformations of polymers [8] and peptides [9]. Jarrold and Bower have worked with an analogous tandem quadrupole setup which incorporates an intermediate 76 mm drift cell [10,11].

In recent years, Jarrold and co-workers [12] have developed high resolution drift cell experiments where the first mass spectrometer is omitted and the ions are produced directly in the drift cell. This has the advantage that the significant loss of ion intensity encountered upon injection into the cell is prevented and this in turn allows to operate at higher cell pressures (up to and above 1 atm), which corresponds to a higher resolution in the mobility measurement (in the range of 100). They applied this technique to a large variety of different ionic systems such as fullerenes and fullerene derivatives [12–16], biopolymers [18–20], silicon clusters [21] and a variety of metal clusters [22–24].

In another setup, Clemmer and co-workers have more recently used an ion trap to accumulate and concentrate the ions before injection into a drift cell (400 mm long, up to 400 mbar, resolution up to 170). This is followed by a time-of-flight mass spectrometer (TOFMS) [25,26]. This setup has been optimized for rapid data acquisition, i.e., time-of-flight mass spectra and drift time distributions are recorded simultaneously. It allows rapid screening of (for example) peptide libraries [25,26], the unfolding reactions of peptides [27] and the analysis of the size parameters of the various amino acids in peptides [28].

A possible drawback of the latter two approaches (i.e., without mass selection in front of the cell) is that the mass of the investigated ion is determined only after the drift cell and one therefore, cannot strictly rule out fragmentation processes in the drift cell. For this reason, we decided to keep the first mass separation step and optimized the drift cell relative to a typical 40 mm configuration as used by Kemper and Bowers [6] to increase the resolution combined with high throughput. The key difference compared to the above mentioned setups is that our instrument uses a TOFMS to select the desired ion mass *prior* to injection into the drift cell. We consider this to be an ideal combination between a pulsed ion source and a mobility experiment since the TOFMS produces short

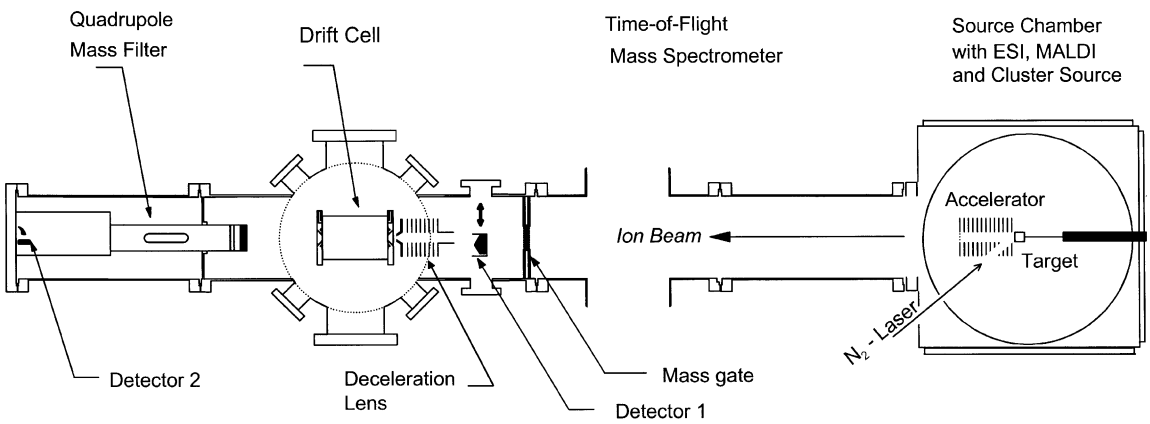

Fig. 1. Instrument overview: the instrument comprises a TOFMS and a quadrupole mass filter coupled to an ion mobility cell. The source chamber contains three different flange mounted ion sources: an electrospray ionization source (ESI), a matrix-assisted laser desorption/ionization source (MALDI), and a Smalley type cluster source.

(<1 μs), intense pulses of mass selected ions that are ideal for the subsequent drift time measurement. [1] The drift cell is a helium filled glass cylinder. It is followed by a quadrupole mass filter for mass analysis. Fig. 1 shows an overview of the instrument.

2. Experimental setup

2.1. Overview

We are currently using three different interchangeable ion sources: a matrix-assisted laser desorption/ionization (MALDI) source, an electrospray ionization source (ESI) and a Smalley/deHeer type [30] laser vaporization cluster source. The ions are typically accelerated to 5 kV in the source region of the TOFMS. An auxiliary detector can be positioned into the beam path close to the entrance of the drift cell. It allows us to control and optimize the source conditions (intensity, mass distribution) prior to injection into the drift cell. A crucial part of the experiment is the pulsed mass gate that removes all unwanted ions by an electrostatic throw-out process within the TOFMS flight tube. The mass gated ion beam is decelerated with a pulsed lens to energies in the range between 50 and 5 keV (lab frame) and injected into the drift cell. This cell is 110 mm long and consists of a double-walled glass cylinder that can be cooled to 100 K and heated up to 500 K. A series of guard rings connected with a resistor chain (200 kΩ, Caddock) generates a homogenous electrical field across the cell. The cell pressure is adjustable in the range between 1 and 25 mbar. A quadrupole mass filter behind the cell enables us to separate and analyze possible fragment ions.

2.2. Ion sources and first mass spectrometer

The source chamber is a 400 mm × 400 mm × 400 mm stainless steel cube with 350 mm ports on each face. It contains the acceleration stage of the TOFMS and the three ion sources (see Fig. 2). The chamber is pumped by a 6000 l/s VHS-10 diffusion pump backed by an Edwards E1M80 80 m^3/h forepump. It can be separated from the main chamber and the pump by two gate valves—this allows us to have a quick access to the ion sources for cleaning and maintenance.

2.2.1. Cluster source

The cluster source is a variant of a Smalley type setup with a rotating rod target, pulsed valve to provide the cooling gas and supersonic expansion through a conical nozzle. The source block design is extremely simple (see Fig. 2): it basically consists of two bores perpendicular to each other: one, 6 mm wide, to house the target rod and the other one 2 mm wide for the cooling gas. This bore opens to a 10 mm wide and 10 mm long hole that serves as a condensation region for the clusters before they leave the block through a nozzle. Attached to the back side of the block is a pulsed valve (General Valve Corp.) that injects the cooling gas (Helium, backing pressure 5–10 bar) around the target rod into the source block. The vaporization laser (Continuum-ND 61, second harmonic, 532 nm, 30 Hz) is focused through the nozzle onto the target rod. With the current setup we can use target rods with diameters between 3 and 5 mm. The rod is mounted between two 6 mm diameter teflon cylinders. They serve as gaskets and prevent leakage of the cooling gas pulse (cf. Fig. 2). The complete gasket-rod-gasket assembly is translated and rotated with a screw mechanism mounted on a motor driven rotary feedthrough. The comparatively tight source block design results in good clustering conditions with a source chamber pressure in the low 10^{-4} mbar range. We use different types of nozzles depending on the system we investigate—the gold cluster cation mobility data (Fig. 9) were obtained with a nozzle with an inner diameter of 1 mm and a conical angle of 30°. The clusters formed in the source block under these conditions are expanded through the nozzle into the source chamber. They drift for 40 mm guided by an electrostatic lens into the accelerator of the

[1] A comparable instrument with a MALDI source/reflectron/drift cell combination has recently been realized by Kemper and Bowers [29].

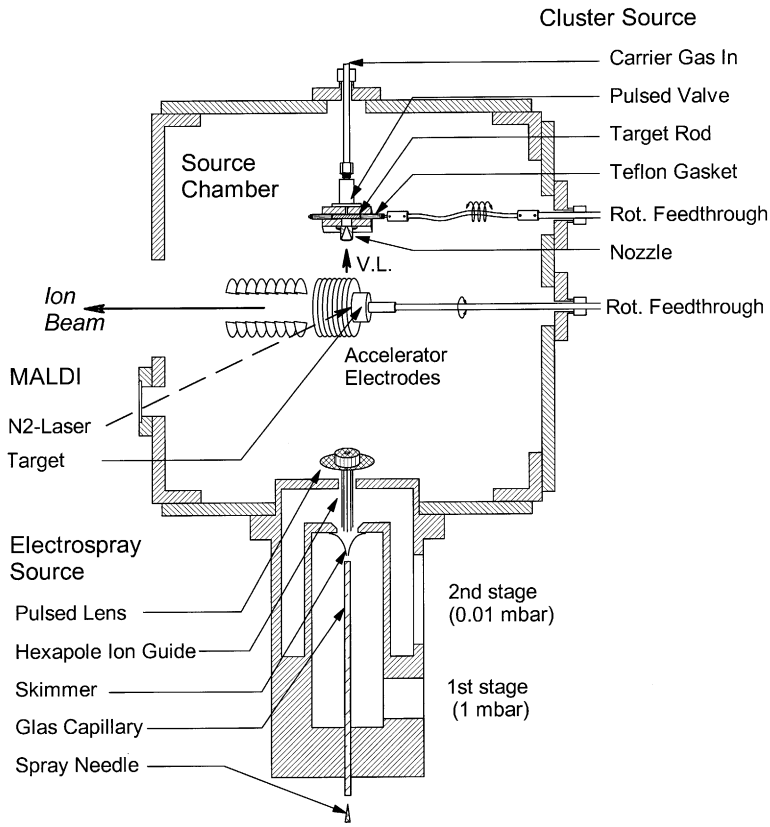

Fig. 2. ESI, MALDI and laser vaporization cluster sources: the electrospray (ESI) and cluster source are both mounted on a 350 mm diameter flange, whereas the MALDI source is directly mounted on the accelerator of the TOFMS. When operating the cluster source we replace the flange with the ESI source by a viewport in order to focus the vaporization laser onto the target. VL: vaporization laser (Nd–YAG, 532 nm).

TOFMS. The accelerator is typically first at ground potential until the cluster ion packet in the primary ion beam passes into the extraction volume. It is pulsed to 5 kV within 200 ns with a fast high voltage switch (Behlke). The cluster composition depends critically on the timing between pulsed valve (t_0), vaporization laser ($t_0 + 500 \cdots 1500\,\mu s$) and acceleration pulse ($t_0 + 1000 \cdots 2000\,\mu s$).

2.2.2. MALDI-source

The MALDI-source consists of a rotating target disk, mounted directly onto the repeller plate of the mass spectrometer. The target is a polished stainless steel disk with a diameter of 10 mm. The sample/matrix mixture is spin coated onto the disk. A N_2-laser (MSG 405 TD, Laser Technik Berlin) with up to 200 μJ per pulse (pulse length 500 ps) is used for desorption and ionization. The laser is incident at an angle of 45° and focused onto the target with a 300 mm focal length lens (≈0.5 mm^2 spot size). The pulse energy is adjusted with a pair of quartz deflection plates. Typical pulse energies are 50 μJ, repetition rates are in the range of 30 Hz. In order to improve the mass resolution, the acceleration field is off when the laser fires, it is pulsed to 5 kV typically 1–20 μs after the laser pulse.

2.2.3. Electrospray-source

Electrospray ionization has proven to be an extremely powerful technique to bring non-volatile

molecules into the gas phase primarily out of polar solutions. An electrospray-source generally consists of a "sprayer", i.e., a tip or needle that disperses the analyte solution into fine droplets. The second step is the transfer into the vacuum system that usually requires a capillary and several stages of differential pumping. In our setup, we are using a commercial off-axis sprayer (Analytica of Branford, Model #105231-M) that enhances the spray process with the help of a flow of nebulizing gas (N_2) flowing axially around the needle. The charged droplets drift through a flow of drying gas (N_2) into a glass capillary (0.5 mm, 250 mm long) which serves to transfer the ions from ambient pressure into the first pumping stage (see Fig. 2). Both ends of the capillary are metalized, the front end is typically at 5 kV (positive for anions, negative for cations), the back end 100–300 V above ground. This first stage is pumped by a Leybold Trivac S65B rotary pump to a pressure of 1 mbar. The ions exiting the capillary pass through a skimmer (Beam Dynamics) into the second stage of differential pumping, with a pressure of 8×10^{-3} mbar, obtained by an Edwards EXT255H turbo pump. The inner diameter of the skimmer is 2 mm and it is located 5 mm downstream from the capillary exit. The skimmer potential is between the capillary exit potential and ground level, so that the ions are focused into the skimmer orifice. The actual voltage depends on the particular ion and it is a compromise between intensity loss due to diffusion at low voltages and collision-induced dissociation at high voltages. A typical value is 50 V above ground. Immediately following the skimmer is a hexapole ion guide that is operated at a frequency of 3 MHz and RF voltages between 100 and 1000 V_{pp}, depending on the ion mass, plus a dc voltage of typically 5–20 V. It consists of 1.5 mm rods mounted concentrically on a diameter of 5 mm, each having a length of 60 mm and serves to store and transfer the ions into the source chamber. The storage is necessary in order to efficiently couple the continuous electrospray process to the pulsed operation of a TOFMS. It is done by a lens at the exit of the hexapole that is pulsed from a voltage slightly above the hexapole dc voltage (thus, preventing the ions from leaving the hexapole) to typically −10 V. This setup transfers an ion packet into the region between the electrodes of the TOFMS where it is accelerated towards the drift cell.

2.2.4. Time-of-flight mass spectrometer

The TOFMS is a Wiley–McLaren type setup [31] with the acceleration region split in two adjustable fields (repeller at 5 kV, 30 mm long, and extractor at 4.5 kV, 10 mm long). The field-free drift region, i.e., the distance between the accelerator and the (primary) detector is 900 mm long. All unwanted ions are removed by means of a pulsed mass gate, that consists of a stack of closely spaced (2.5 mm) metal strips (0.1 mm thick and 7 mm long)—see Fig. 3a. This mass gate is a variation of the device developed by Weinkauf and co-workers [32] and optimized in our group [33]. For mechanical stability reasons, we are using thin metal strips instead of wires. Adjacent pairs of these strips can be pulsed from ground to up to +800 and −800 V, respectively, with a home built supply (150 ns rise time, 500 ns minimum pulse width). According to SIMION [34] simulations the deflection angle for 5 keV ions is 20°, sufficient to prevent the ions from reaching the detector and the entrance of the drift cell (Fig. 3b). To isolate an ion packet the field is switched off during the time the packet passes this region. Fig. 3c shows an example—C_{84}^+ isolated out of a beam of different fullerene ions made by laser desorption.

The mass selected ion beam is decelerated with a pulsed electrical field (see Section 2.2.7) and focused into the ion mobility cell. Typical injection energies are in the range of 100 eV (lab frame), which corresponds to less than 0.5 eV center of mass energy for ions above 1000 amu (helium as buffer gas). An efficient focusing is essential since the entrance aperture of the drift cell has a diameter of 0.5 mm. This size is ultimately limited by the buffer gas pressure in the cell, which is currently up to 20 mbar, and the pumping speed available in the main chamber, which is 2000 l/s (Edwards Diffstak 250/2000C).

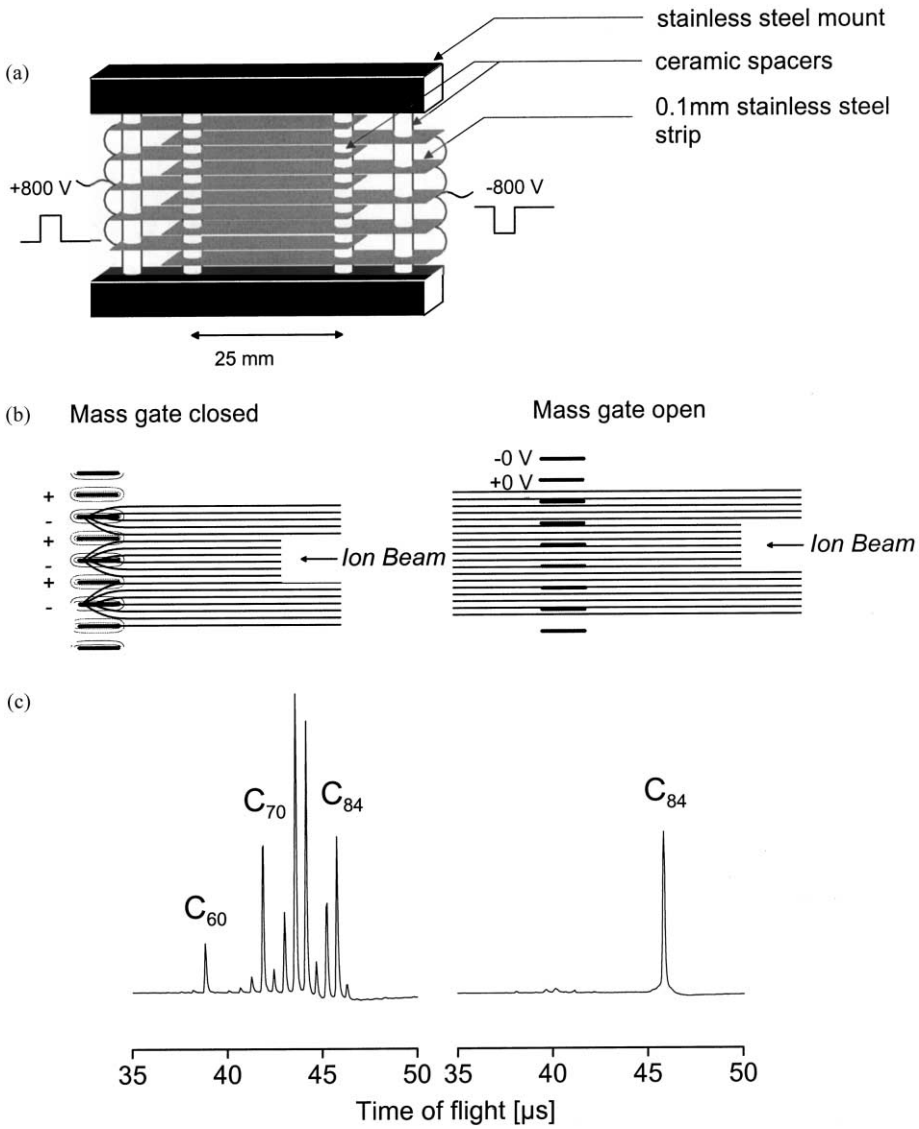

Fig. 3. (a) Mass gate assembly: the gate consists of a stack of 0.1 mm thick and 7 mm wide stainless steel strips with a 2.5 mm spacing. (b) SIMION calculation of the trajectories of cations (1000 amu, 3 keV kinetic energy) passing the mass gate. Mass gate closed: alternating electrodes are at potentials of exactly (within 1%) the same magnitude but opposite polarity, typically ±800 V. All the ions passing the gate are strongly deflected and collide with the electrodes. Mass gate open: the electrodes are shorted to ground. (c) Selection of C_{84}^+ from a fullerene mixture.

2.2.5. Ion mobility cell design

The goal of the experiment is to measure the transit time of the ions through the cell under the influence of an applied electrical field. This time is connected with the (reduced) ion mobility K_0 by [5]

$$K_0\,(\mathrm{cm}^2/\mathrm{V\,s}) = \frac{L}{t_\mathrm{D} E_\mathrm{D}} \frac{P}{1013\,\mathrm{mbar}} \frac{273.2\,\mathrm{K}}{T} \qquad (1)$$

where L is the length of the drift tube and E_D the applied drift field, P the buffer gas pressure in mbar, and T its temperature in Kelvin. In this experiment, the tube

length is 110 mm, the He pressure is in the range between 1 and 25 mbar, and typical field strengths are in the range between 2 and 30 V/cm. This is well within the so-called low-field limit—the diffusive drift motion of the ions is only slightly perturbed by the superimposed electrical field. This also means that there is no alignment of the ions relative to the field. Under these conditions, the mobility of an ion is independent of the applied electrical field. In other words, if we measure the drift time t_D as a function of applied field, pressure, and temperature, we obtain the mobility of the ion. In practice, the best procedure is to keep temperature and pressure constant and to vary the field across the cell. The mobility of an ion can then be obtained from the slope of a plot of the arrival time vs. the drift voltage. According to kinetic theory it can be connected with the collision cross section Ω [5]:

$$K_0\,(\mathrm{cm}^2/\mathrm{V\,s}) = \frac{3q}{16N_0}\sqrt{\frac{2\pi}{\mu k_B T}}\frac{1}{\Omega} \qquad (2)$$

where q is the charge, N_0 the number density of helium and μ is the reduced mass of the ion and helium. When injecting ions into a gas filled drift cell with tens of eV of injection energy, these ions will travel a couple of millimeters before they are thermalized by the collisions with the buffer gas. In order to minimize this entrance effect, we use a constant field of typically 50 V/cm across the first 5 mm of the cell (Fig. 4—"entrance field"). The rest of the cell is separated by a grid, and it is this field that is varied in order to measure the mobility (Fig. 4—"drift field"). The last part of the cell (Fig. 4—"focus field" and "exit field") contains a focusing lens that directs the ions toward the exit aperture (0.5 mm) of the drift cell, it represents an improved version of a device first implemented by Kemper and Bowers [35]. This focusing element leads to an increase in intensity of a least one order of magnitude, as can be seen from a SIMION calculation (Fig. 5). The ion motion is calculated according to the

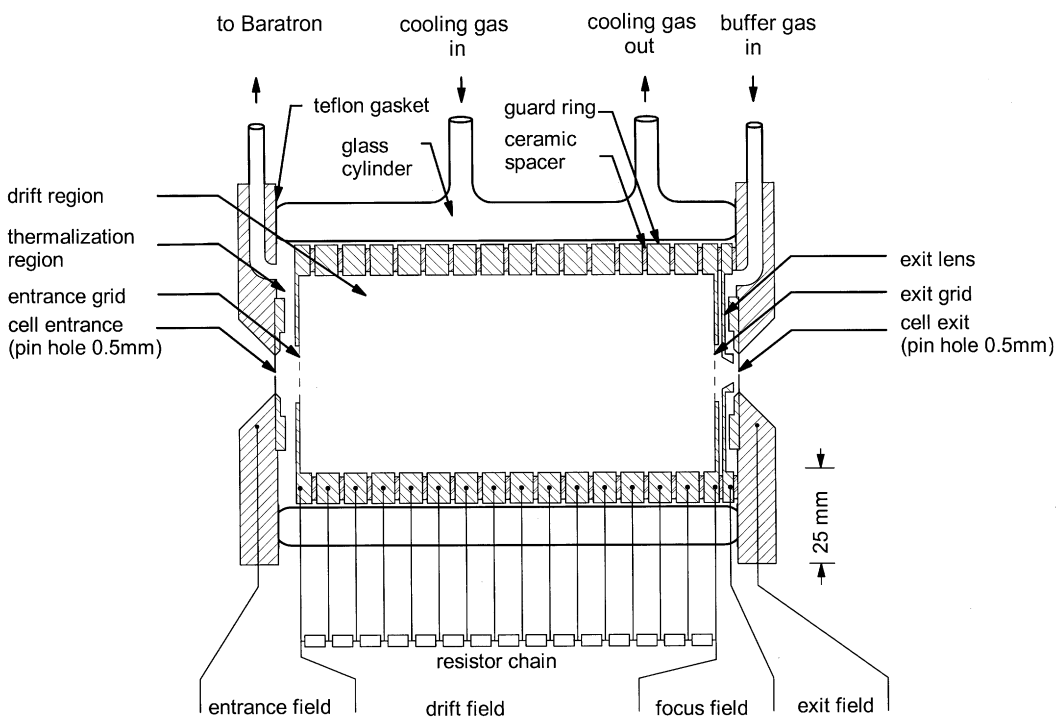

Fig. 4. Schematic of the ion mobility cell. The cell consists of a double walled glass cylinder with copper end caps on both sides. The ions enter end leave the cell through 0.5 mm diameter pin holes. The cell comprises four regions within which the electrical field can be independently adjusted, the entrance, drift, focus and exit field. For details see text.

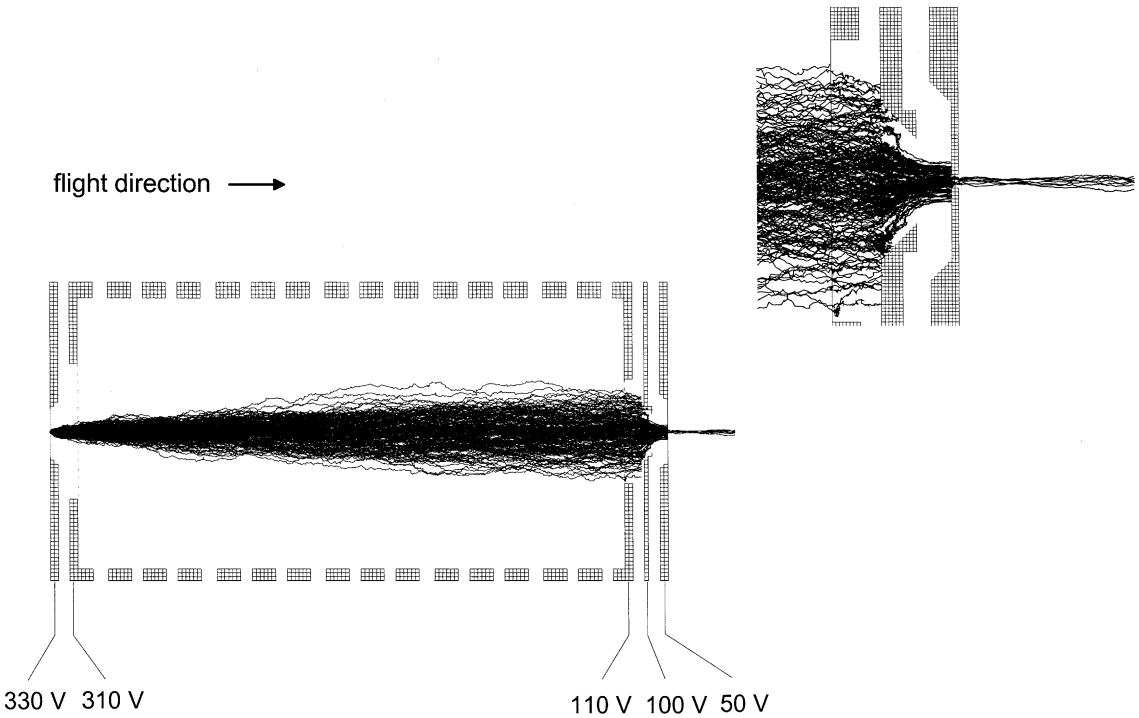

Fig. 5. SIMION simulation of the drift motion in the cell and the effect of the focusing lens (see text for details). The conditions for the simulation are cell pressure 7 mbar, ion mass 500 amu, cell temperature 300 K. Under these conditions roughly 1% of the ions finally escape through the exit hole (0.5 mm).

electrostatic fields combined with a damping factor (proportional to the buffer gas pressure and inversely proportional to the mobility of the ion, its mass and the buffer gas temperature) and a random hopping according to the Stokes–Einstein equation. Note, however, that even with this focusing lens more than 99% of the ions are lost within the cell due to collisions with the walls.

The cell consists of a double walled glass cylinder that is 120 mm long, and has an inner diameter of 70 mm and an outer diameter of 95 mm. The space between inner and outer wall is connected via a LN_2-feedthrough to a temperature control system (outside the vacuum) that allows us to blow cool (down to 77 K) or warm (up to 500 K) nitrogen gas through the cylinder. Both ends of the cylinder are sealed by copper end plates with 0.2 mm teflon foil as a gasket. They are pressed against the glass cylinder by a set of eight molybdenum threaded rods (these have basically the same coefficient of thermal expansion as the glass used for the cylinder). The copper end plates are also connected to the temperature control system by a set of feedthroughs for each plate, and the gas flow can be adjusted by needle valves. The temperature inside the cell is monitored by two PT100 thermistors immersed in the buffer gas and additionally by two K-type thermocouples attached to the copper entrance and exit plates.

The electrical drift field inside the cell is established by a stack of 15, 6 mm thick, 52 mm inner diameter copper guard rings separated by 1.27 mm thick ceramic spacers. They are connected by a chain of 14, 200 kΩ resistors (Caddock). The pressure is monitored with a MKS 627B baratron capacitance manometer which has a specified accuracy of 0.15%.

2.2.6. Quadrupole mass spectrometer

The connection between the main chamber and the detector chamber is via the 4 mm entrance aperture of the quadrupole mass spectrometer. This chamber is pumped by a Varian V550 turbomolecular pump (500 l/s). Its pressure is typically in the 10^{-7} to 10^{-6} mbar range, depending on the gas load in the main chamber. The transfer from the exit orifice to the entrance of the quadrupole is via a set of three electrostatic lenses. The quadrupole is an Extrel C50 system with *m*/*z* range of 0–5000 amu, modified so that the mass scan is under computer control. The detector is a Model # 402A channeltron (Detector Technology Inc.). The signal from the detector is fed into an EG&G MCS-board (2 μs minimal dwell time). When determining the drift time of a particular ion, the mass filter is set to the respective mass and the MCS-board is triggered synchronously with the deceleration voltage pulse. A typical drift time distribution has a length of 1–5 ms, depending on the ion mobility and the applied pressure and drift voltage. In a different mode, the quadrupole mass filter also allows us to measure the fragment distribution resulting from collision-induced dissociation by high energy injections into the cell. Under these conditions the mass filter scan and the MCS-board are synchronized so that each channel corresponds to a particular mass. The channels are advanced with each laser shot until the mass scan is complete.

2.2.7. Electrical setup

Since it is difficult to float the quadrupole mass filter by more than ±100 V, we keep this potential close to ground. The cell exit is at 5–50 V higher—this defines the energy of the ions entering the quadrupole. The drift cell "focus" is typically another 100 V above the exit, the "drift" voltage 100–500 V further up, and the cell "entrance" 20–50 V above the "drift" voltage (cf. Figs. 4 and 5). In a drift time experiment, the arrival time is measured as a function of the field in the drift region ("drift field"). It is essential that when changing this field the other fields remain constant. Therefore, all the respective power supplies float on top of each other. It is also essential that the injection energy can be varied independent of the voltages in the cell in order to investigate fragmentation or isomerization reactions as a function of the collision energy. A possible approach would be to vary the acceleration energy, i.e., the energy the ions obtain in the TOFMS accordingly. This setup has two serious drawbacks however: firstly the transfer efficiency of the TOFMS strongly decreases below 2000 V acceleration voltage and secondly one would have to adjust the mass gate timing for each voltage change. Therefore we chose to keep the acceleration voltage fixed (at 5 kV) and decelerate the ions shortly before injection in a pulsed field. This deceleration setup basically consists of a 40 mm long 20 mm i.d. isolated tube with both ends covered with a nickel mesh (Buckbee Mears, MN-20) in order to minimize field penetration. The tube potential is at ground until the ion packet has passed the entrance grid of the tube. Within 200 ns it is pulsed to the desired deceleration voltage and the ion packet leaving the tube experiences a strong deceleration field in the region between the exit of the tube and the cell entrance. A set of static lenses focuses the beam to the entrance aperture of the cell.

3. Results

3.1. Fullerenes and fullerene derivatives

We have measured the mobilities of C_{60}^+ and a series of larger fullerenes, such as C_{70}^+, C_{76}^+, C_{78}^+, and C_{84}^+. These ions are produced by laser desorption/ionization of a fullerene mixture sample with the N_2 laser in our MALDI source but without a matrix substance added. This can be considered as a calibration measurement since the structures of these molecules are well known both in the condensed phase and for C_{60} and C_{70} in gas phase. There have also been mobility measurements of cations and anions by different groups [7,13–17,36] which have confirmed the gas phase fullerene structures. Fig. 6a shows an example of a drift time distribution of C_{60}^+ at a cell pressure and temperature of 6.2 mbar and 300 K, respectively. The corresponding drift voltage was 300 V.

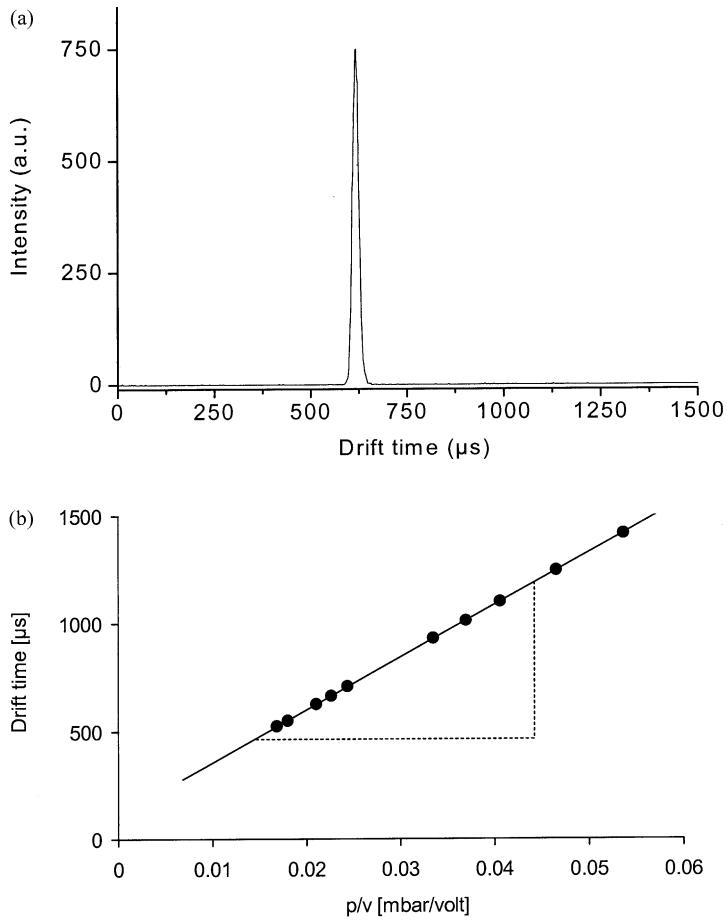

Fig. 6. (a) Drift time distribution of C_{60}^+. The pressure was 6.2 mbar, drift voltage 300 V, temperature 300 K. From the ratio of peak width and drift time we obtain a resolution ($t/\Delta t$) of 30. The count rate is in the range of 1000 cps, i.e., the measurement took less than 10 s. (b) Illustration of how to obtain the mobility from the slope of the drift time vs. applied drift voltage (at constant pressure, 2.1 mbar in this case).

The resolution can be determined as the ratio of the drift time and the peak width (full width at half maximum, $t/\Delta t$), we obtain a value of 30. From the slope of a plot of drift time against the ratio of drift voltage and cell pressure we get the ion mobility (cf. Fig. 6b). The accuracy of the determined mobility depends on several parameters: firstly, the quality of the fit, i.e., the linearity of the t vs. p/v plot. We typically obtain an uncertainty in the slope which is in the range of 1% or lower. Secondly, the precision of the pressure measurement, which, according to the calibration of the baratron, is better than 0.25%. Thirdly, the accuracy of the different voltages. As mentioned above, a variation of the drift voltage requires a variation of the cell entrance voltage and also of the pulsed deceleration voltage in order to keep the corresponding electrical fields constant. We estimate these errors to be in the range of 0.5%. This amounts to a total uncertainty of our mobility measurement of less than 2%.

From the mobility data, we obtain the collision cross sections according to Eq. (2). Such experimental collision cross sections can be directly compared with cross sections obtained by theoretical methods. The latter may be determined to various possible levels of

sophistication, such as the projection approximation (see, for example [37]), the exact hard spheres scattering model [38], and trajectory calculations [39]. In this example, we are using the simplest approach, the projection approximation, which treats the interaction of the ion and the helium atoms as a collision of hard spheres and approximates the collision cross section by the surface area of the hard spheres molecule. Given a quantum-chemically determined molecular structure, the only adjustable parameters in this model are the hard sphere atomic radii of the constituents of the ion and of helium.

Fig. 7 summarizes the measured and calculated cross sections for the different fullerene cations and also of some derivatives such as fullerene oxides and oxide dimers which we have studied. The latter derivatives were produced in our laboratory by a reaction of C_{60} with $C_{60}O$ ($\rightarrow C_{60}OC_{60}$), C_{70} with $C_{70}O$($\rightarrow C_{70}OC_{70}$), and $C_{60}O$ with C_{70} ($\rightarrow C_{70}OC_{60}$) [40] purified by HPLC and brought into the gas phase with MALDI (matrix: 9-nitroanthracene, 100/1). They consist of two fullerene cages connected by a five-ring furane-like bridge. Their structures have been indirectly confirmed by a comparison of the measured characteristic low frequency Raman active vibrational modes with PM3 calculations. The structure of $C_{60}OC_{60}$ in condensed phase has been confirmed by ^{13}C NMR spectroscopy [41]. $C_{70}OC_{60}$ has five possible isomers, three of these have been isolated and characterized in our lab. We investigated the C_1 isomer [42]. In the case of $C_{70}OC_{70}$, we used a mix of different isomers. Our mobility measurements

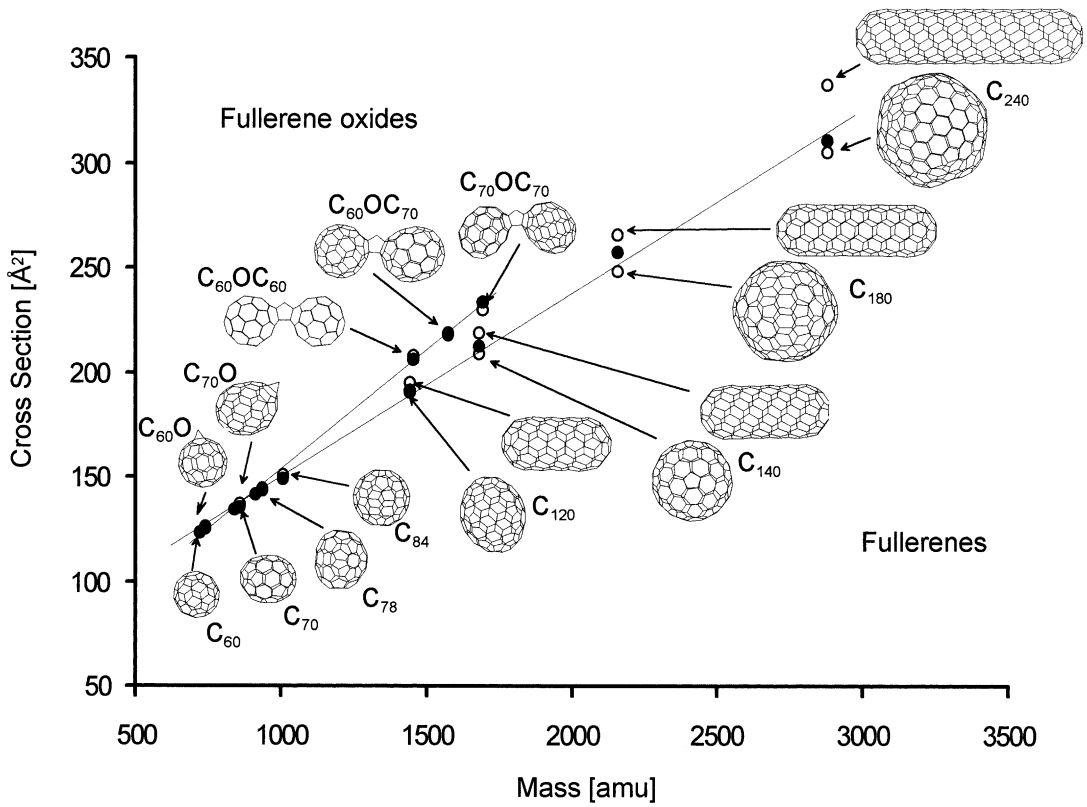

Fig. 7. Experimental and calculated cross sections of some fullerene and fullerene oxide cations. The solid circles indicate the experimental data, the open circles results from calculations. The structures are obtained from PM3 calculations. The cross sections scale linearly with the cluster size which is consistent with hollow spheres.

agree within the experimental error (2%) with these proposed oxygen-bridged dumbbell structures (based on simulated mobilities using computationally derived PM3 equilibrium structures and the projection approximation).

It should be mentioned that these fullerene oxides are quite fragile under laser irradiation—upon laser desorption they easily fragment into the respective fullerene monomers and at higher laser fluences they undergo coalescence [43] readily losing O, C_2O (plus several C_2 units) to form pure carbon clusters. The mass spectrum obtained under high desorption fluence conditions (without MALDI matrix) therefore, contains a series of coalescence peaks spaced by C_2 units. We focused on C_{120}^+, C_{140}^+, C_{180}^+, and C_{240}^+. Comparison between measurement and simulated ion mobilities for various candidate structures clearly shows that these oxygen-free carbon clusters have a structure that consists of only one, large fullerene-like cage. In other words, the laser irradiation and subsequent

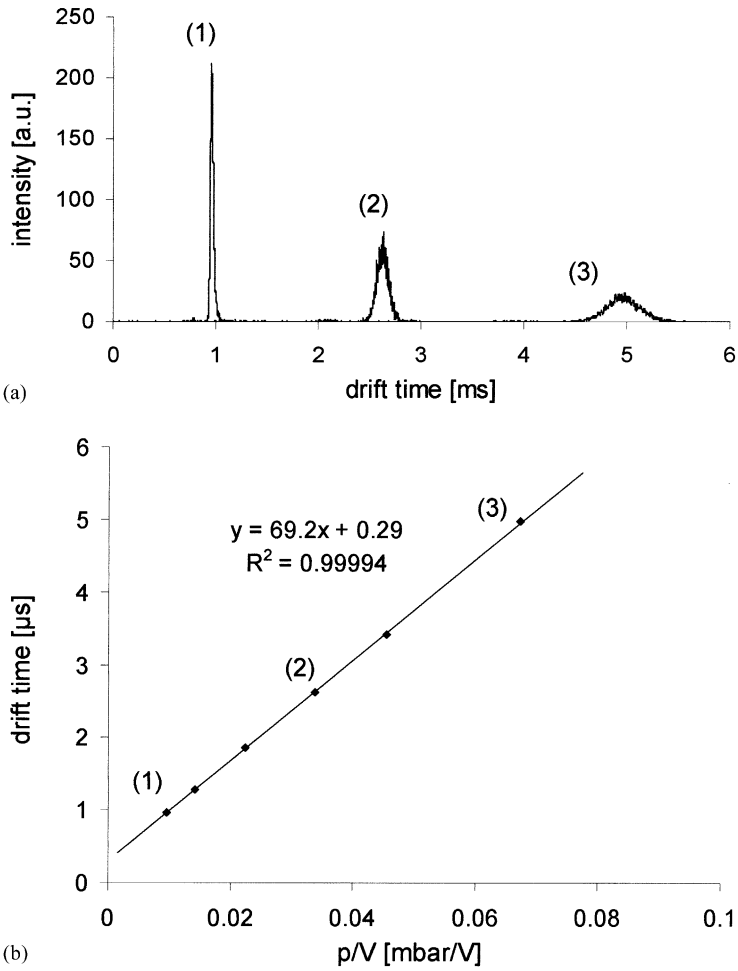

Fig. 8. (a) Drift time distribution of $Au_{13}Se_6(dppe)_6^+$. The pressure was 3.4 mbar, drift voltage 350 V (1), 100 V (2), and 50 V (3), temperature 300 K. The count rates were 200 cps at the highest voltage and 50 cps at the lowest. In other words, the measurement of the whole data series took less than 10 min. (b) Drift time vs. applied drift voltage—the linearity of the fit is extremely good and allows us to determine the cross section even for these large systems to within 2%.

oxygen loss leads to a rearrangement reaction that fuses the two smaller fullerene cage into one large cage structure. In the simulations, we have specifically compared dumbbell structures with several kinds of closed shell forms, especially an almost spherical isomer and a capped nanotube. While dumbbells are clearly not observed, cross sections of both kinds of closed shell structures agree with the experimental data to within the experimental errors. However, in general, the agreement with the more spherical candidate structure is somewhat better. While we do not observe structured drift time distributions as seen for example in [16,17], it should be mentioned that we cannot rule out the *initial formation* of other structures such as dumbbell [2 + 2] cycloadducts or ball and chain dimers [16,17] in the laser desorption process—these isomers are however, known to be significantly less stable than the observed closed shell forms on the basis of various electronic structure calculations. Consequently, if initially present, we might expect them to break apart during injection.

3.2. Ligated gold–selenide clusters

Another test case was a large inorganic cluster with the composition $Au_{18}Se_8(dppe)_6^{2+}$ (dppe = bis(diphenylphosphanyl)ethane). The substance is stable against air and moisture and its structure has been determined by X-ray crystallography [44]. It is soluble in CH_2Cl_2 and can be readily brought into the gas phase by electrospray ionization. We were curious whether it was possible to inject this ion into the drift cell without fragmentation. We find that the majority of the ions survive an injection with low energy (100 eV lab frame) and we obtained a mobility consistent with the solid phase structure. At higher injection energies we find that the cluster ion fragments into two major products, namely $Au_5Se_2(dppe)_2^+$ and $Au_{13}Se_6(dppe)_3^+$. We also measured the mobilities of these fragments (by setting the quadrupole to the respective masses). Calculations to get candidate structures for these fragments that can be compared with the experimental data are underway [45].

As an example of the performance of our instrument we show in Fig. 8 the arrival time distributions of $Au_{13}Se_6(dppe)_3^+$ for three different drift voltages—this ion has a mass of 4200 amu and is at the limit of the range of the quadrupole mass spectrometer. Nevertheless, the transmission of the instrument allowed for count rates well above 100 cps, i.e., a single drift time measurement corresponding to the accumulation of 5000 counts took less than 1 min.

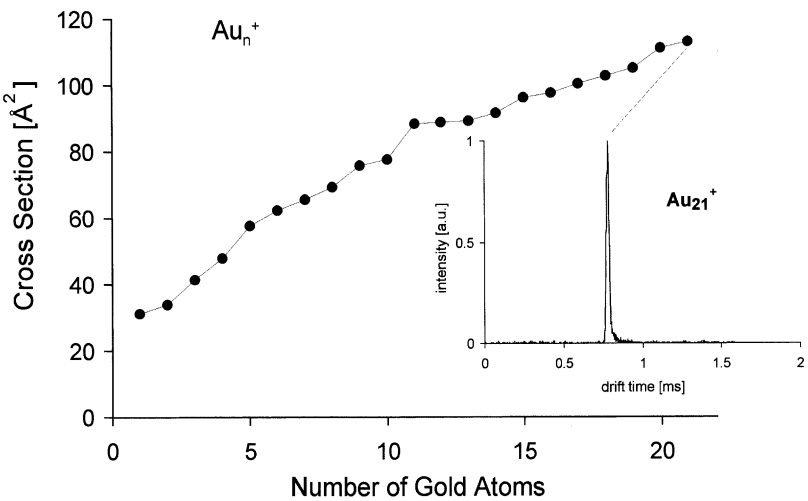

Fig. 9. Cross sections of gold cluster cations as a function of cluster size. Typical statistical errors are in the range of 2%. Inset: drift time distribution of Au_{21}^+ at a pressure of 8.3 mbar, 350 V, 300 K. The count rate is 40 cps, i.e., this measurement took less than 1 min.

3.3. Gold clusters

The structure of bare, ligand-free gold clusters is still subject to controversy in the literature [46–48]. Especially, the question of the size at which (depending on the charge state) these clusters begin to form three dimensional structures is open. With our cluster source we were able to produce positively and negatively charged Au_n ions ($n = 1 \ldots 21$) in high enough intensities to measure their mobilities. The results for the cations are summarized in Fig. 9—together with an example drift time distribution for Au_{21}^+. Calculations to identify the respective structures are underway and will be reported together with more detailed experiments in a future publication [49].

Acknowledgements

This research was supported by the Deutsche Forschungsgemeinschaft. We thank Frank Hennrich (fullerenes and fullerene oxides), Dieter Fenske and Timo Langetepe (gold–selenium clusters) for providing samples.

References

[1] A.G. Marshall, Int. J. Mass Spectrom. 200 (2000) 331.
[2] M.T. Bowers, A.G. Marshall, F.W. McLafferty, J. Phys. Chem. 100 (1996) 12897.
[3] F.W. McLafferty, R. Kornfeld, W.F. Haddon, K. Levsen, I. Sakai, P.F. Bente, S.-C. Tsai, H.D.R. Schuddemage, J. Am. Chem. Soc. 95 (1973) 3886.
[4] K.M. Stirk, M. Kiminkinen, H.I. Kenttämaa, Chem. Rev. 92 (1992) 1649.
[5] E.A. Mason, E.W. McDaniel, Transport Properties of Ions in Gases, Wiley, New York, 1988.
[6] P.R. Kemper, M.T. Bowers, J. Phys. Chem. 95 (1991) 5134.
[7] G.V. Helden, N.G. Gotts, M.T. Bowers, Nature 363 (1993) 60.
[8] G.V. Helden, T. Wyttenbach, M.T. Bowers, Science 267 (1995) 1483.
[9] T. Wyttenbach, G.V. Helden, M.T. Bowers, J. Am. Chem. Soc. 118 (1996) 8355.
[10] M.F. Jarrold, J.E. Bower, J. Chem. Phys. 96 (1992) 9180.
[11] M.F. Jarrold, J.E. Bower, J. Chem. Phys. 98 (1993) 2399.
[12] Ph. Dugourd, R. Hudgins, D.E. Clemmer, M.F. Jarrold, Rev. Sci. Instrum. 68 (1997) 1122.
[13] J. Hunter, J. Fye, M.F. Jarrold, Science 260 (1993) 784.
[14] J.M. Hunter, M.F. Jarrold, J. Am. Chem. Soc. 117 (1995) 10317.
[15] A. Shvartsburg, R. Hudgins, Ph. Dugourd, M.F. Jarrold, J. Phys. Chem. A 101 (1997) 1684.
[16] A. Shvartsburg, M.F. Jarrold, J. Phys. Chem. A 103 (1999) 5275.
[17] A. Shvartsburg, L.A. Pederson, R. Hudgins, G.C. Schatz, M.F. Jarrold, J. Phys. Chem. A 102 (1998) 7919.
[18] K.B. Shelimov, D.E. Clemmer, R.R. Hudgins, M.F. Jarrold, J. Am. Chem. Soc. 119 (1997) 2240 .
[19] J. Woenckhaus, Y. Mao, M.F. Jarrold, J. Phys. Chem. B 101 (1997) 847.
[20] K.B. Shelimov, M.F. Jarrold, J. Am. Chem. Soc. 119 (1997) 2987.
[21] R. Hudgins, M. Imai, M.F. Jarrold, P. Dugourd, J. Chem. Phys. 111 (1999) 7865.
[22] M.F. Jarrold, J.E. Bower, J. Phys. Chem. 97 (1993) 1746.
[23] A. Shvartsburg, M.F. Jarrold, Phys. Rev. Lett. 85 (2000) 2530.
[24] A. Shvartsburg, M.F. Jarrold, Chem. Phys. Lett. 317 (2000) 615.
[25] S.C. Henderson, S.J. Valentine, A.E. Counterman, D.E. Clemmer, Anal. Chem. 71 (1999) 291.
[26] C.A. Screbalus, J. Li, W.S. Marshall, D.E. Clemmer, Anal. Chem. 71 (1999) 3918, and references therein.
[27] J. Li, J.A. Taraszka, A.E. Counterman, D.E. Clemmer, Int. J. Mass Spectrom. 185–187 (1999) 37.
[28] S.C. Henderson, J. Li, A.E. Counterman, D.E. Clemmer, J. Phys. Chem. B 103 (1999) 8780.
[29] P. Kemper, M.T. Bowers, Private communication.
[30] (a) T.G. Dietz, M.A. Duncan, D.E. Powers, R.E. Smalley, J. Chem. Phys. 74 (1981) 6511;
(b) P. Milani, W.A. deHeer, Rev. Sci. Instrum. 61 (1990) 1835.
[31] W.C. Wiley, I.H. McLaren, Rev. Sci. Instrum. 26 (1955) 1150.
[32] U. Boesl, K. Walter, R. Weinkauf, E.W. Schlag, US Patent No. 5032722 (1991), German Patent No. DE 3920566 C2 (1993).
[33] C.W. Stoermer, S. Gilb, J. Friedrich, D. Schoss, M.M. Kappes, Rev. Sci. Instrum. 69 (1998) 1661.
[34] D.A. Dahl, SIMION 6.0, Idaho National Engineering Laboratory.
[35] P. Kemper, M.T. Bowers, Private communication.
[36] N.G. Gotts, G.V. Helden, M.T. Bowers, Int. J. Mass Spectrom. Ion Processes 150 (1995) 217.
[37] G.V. Helden, M.-T. Hsu, N. Gotts, M.T. Bowers, J. Phys. Chem. 97 (1993) 8182.
[38] A. Shvartsburg, M.F. Jarrold, Chem. Phys. Lett. 261 (1996) 86.
[39] M.F. Mesleh, J.M. Hunter, A.A. Shvartsburg, G.C. Schatz, M.F. Jarrold, J. Phys. Chem. 100 (1996) 16082.
[40] H. Eisler, F.H. Hennrich, E. Werner, A. Hertwig, C. Stoermer, M.M. Kappes, J. Phys. Chem. A 102 (1998) 3889.
[41] S. Lebedkin, S. Ballenweg, J. Gross, R. Taylor, W. Krätschmer, Tetrahedron Lett. 36 (1995) 4971.
[42] F. Hennrich et al., in preparation.
[43] R.D. Beck, C. Stoermer, C. Schulz, R. Michel, P. Weis, G. Bräuchle, M.M. Kappes, J. Chem. Phys. 101 (1994) 3243.

[44] D. Fenske, T. Langetepe, M.M. Kappes, O. Hampe, P. Weis, Angew. Chem. 112 (2000) 1925.
[45] P. Weis, R. Ahlrichs, M.M. Kappes, in preparation.
[46] O.D. Häberlen, S.C. Chung, M. Stener, N. Rösch, J. Chem. Phys. 106 (1997) 5189.
[47] G. Bravo-Pérez, I.L. Garzón, O. Novaro, Theochemistry 493 (1999) 225.
[48] N.T. Wilson, R.L. Johnston, Eur. Phys. J. D 12 (2000) 161.
[49] S. Gilb, P. Weis, F. Furche, R. Ahlrichs, M.M. Kappes, J. Chem. Phys., in press.